Hindawi Publishing Corporation
Mathematical Problems in Engineering
Volume 2010, Article ID 726843, 12 pages
doi:10.1155/2010/726843

Research Article

The Effects of Structure Defects on the Performance of a Micro Comb Resonator

D. Guo and Y. Zhu

State Key Laboratory of Tribology, Department of Precision Instrument, Tsinghua University, Beijing 100084, China

Correspondence should be addressed to D. Guo, guodan26@tsinghua.edu.cn

Received 26 November 2009; Revised 12 April 2010; Accepted 1 May 2010

Academic Editor: Irina N. Trendafilova

A micro comb resonator loaded by alternating electric field is modeled by finite element method, The damping is analyzed by both Couette flow model and Stokes flow model. Structure faults are researched its effects on the dynamic characteristics of the micro comb resonator. The result shows that adhesion fault makes the resonance frequency higher and sensitivity reduction, while crack fault debases the resonance frequency and amplitude. When the crack is located near the end, the stress concentration at the crack location is highest, which is easy to induce the support beam broken.

1. Introduction

With the fabrication processes trending to be more mature, the requirement of reliability and production ability of MEMS increases more. Relative to design, the problems during MEMS fabrication process, especially the problems of defect and fault are serious, which will been the bottleneck of MEMS application. So, simulations and experiments of the movement for microdevices with defects are necessary. Using the stable model of fault and testing method to detect the fault, the quality and reliability of MEMS products can be improved. There are many sources for MEMS defects, such as particle contaminants, adhesion, undersigned bend, insufficient or excess etch, sidewall inclination, and notching [1]. In recent years, the fault simulation of MEMS has been investigated by some researchers. An MEMS affected by particulate contaminations was simulated by Deb and Blanton, the relationship between defect location and performance parameter of structure was analyzed [2]. The structure fault of MEMS was also modeled and simulated by Reichenbach et al. [3]. The broken beam fault and unwanted anchor fault of a micromirror were simulated by Chen et al. [4]. The fault-based testing technology for MEMS was illustrated by Mir et al. [5].

Electrostatic-comb structure has been successfully applied to many microsystems such as microsensors, microaccelerometers, microdrives, due to its simple structure and superior performance [6]. The motion of the devices is greatly influenced by fabricating error, variety of parameters, and deformation as well, especially the faults of structure, which make the kinetic accuracy become reduced [7–9]. In this paper, a dynamic model is built to research the dynamic performance of microcomb resonator under alternating electric field, in which both Couette flow model and Stokes flow model are applied to the damping. Structures with point adhesion or beam crack are analyzed for the dynamic characteristics using finite element method.

2. Dynamic Model of a Microcomb

A typical microcomb resonator usually has two sets of fingers, the one which is connected to the substrate is called fixed fingers (or stationary electrode), and the other which is released from the substrate is called movable fingers (see Figure 1). When two different voltages are applied to these two sets of fingers, the resulting electrostatic force drives the movable fingers toward or apart from the fixed ones. When an alternating voltage is applied, the movable electrode oscillates under the electrostatic force and elastic restoring force, which can be designed for a resonator.

Figure 1 shows the schematic of a typical microresonator. Its finite element dynamic equation is:

$$[M]\{\ddot{u}\} + [C]\{\dot{u}\} + [K]\{u\} = \{F\}\sin\omega t \tag{2.1}$$

where $[K]$, $[M]$ is the structural stiffness matrix and mass matrix, which can be obtained by finite element method. $[C]$ is the air damping matrix, which will be derived later. $\{u\}$ is the node displacement vector. $\{F\}$ is the electrostatic force, which can be derived by the finite element method of electrostatic field. ω is the alternating frequency of electric field.

The electrostatic potential in uniform medium has

$$\nabla^2 V = 0 \tag{2.2}$$

where V is the distribution of electric potential. Equation (2.2) is called Laplace Equation. In the Cartesian coordinate, (2.2) can be write as

$$\frac{\partial^2 V}{\partial x^2} + \frac{\partial^2 V}{\partial y^2} + \frac{\partial^2 V}{\partial z^2} = 0 \tag{2.3}$$

when the V is solved from (2.3), the electric field intensity vector $\{E\}$ can be attained from:

$$\{E\} = -\nabla V. \tag{2.4}$$

Then, the electrostatic force on the movable finger has:

$$F = \varepsilon \int_s (\nabla V)^2 ds \tag{2.5}$$

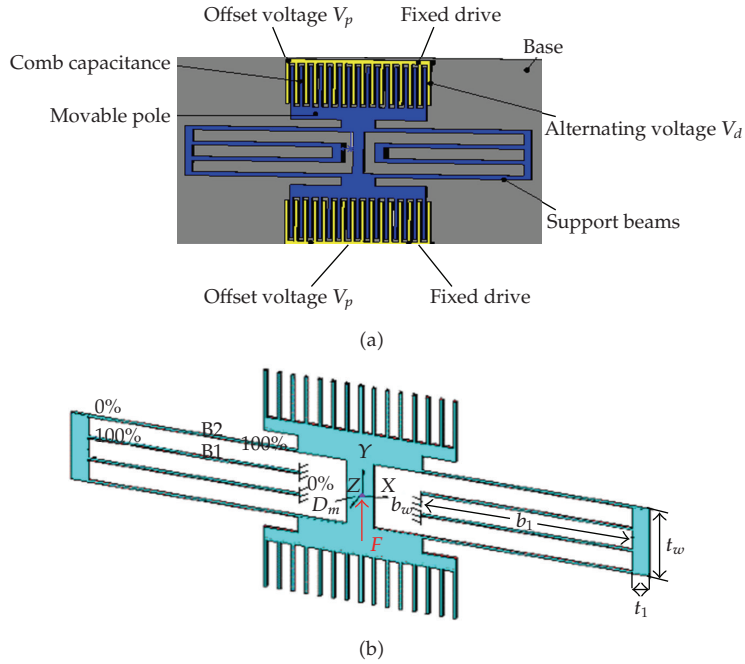

Figure 1: Schematic of microcomb resonator.

where S is the surface of movable finger, and the ε is dielectric coefficient of air, which is 8.854×10^{-6} pF/μm.

The finite element method is applied to analyze the electrostatic field and comb structure. 4-node tetrahedral elements are used to generate meshes. For electrostatic field, the electric potential V at any point can be written as:

$$V = [N]^T [V_e] \tag{2.6}$$

where $[N]$ is the shape function matrix. $[V_e]$ is the node electric potential. According to the principle of minimum potential energy, we have

$$\left\{ \frac{\partial U}{\partial V_e} \right\} = 0 \tag{2.7}$$

where

$$U = \frac{1}{2} \varepsilon \iiint (\nabla V)^2 dx\, dy\, dz. \tag{2.8}$$

Substituting (2.6) into (2.8), combining with (2.7), adding the electric field boundary condition, the $\{V_e\}$ can be solved. Then from (2.5) and (2.6), the electrostatic force at any point can be obtained. For the comb structure, 4-node tetrahedral elements are also used. The electrostatic force is substituting into (2.1), then the subspace iterate method was used

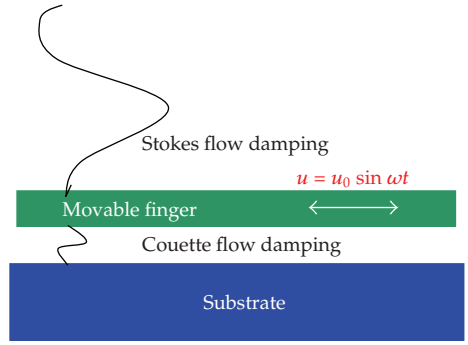

Figure 2: The sketch of damping model.

to obtain the natural frequency and the Newmark integral method was used to obtained vibration response.

Air damping is crucial to the dynamic characteristics of microcomb resonator. For the laterally oscillating resonator, the slide film damping is more significant than the squeeze film damping. So, only the slide film damping is considered here. The air damping of the comb can be divided into three parts, air damping layer (a) between the movable fingers and the base, (b) between the fingers and (c) above the movable fingers. Figure 2 shows the sketch of damping model. For the (a) and (b), air layers are only several microns, so the Couette flow model was applied [10, 11], the damping coefficients can be written as,

$$C_a = \frac{\mu A}{d},$$
$$C_b = \frac{\mu A_c}{g}. \tag{2.9}$$

Because the Couette flow model does not take the media inertial effects into consideration. It can be used under the assumption that the feature distance $\delta = \sqrt{2\mu/\rho\omega}$ is much larger than the gap d between the plate and the substrate [12]. Where μ is viscosity coefficient of air, $\mu = 0.185 \times 10^{-10}\,\mathrm{kg/s/\mu m}$, ρ is the density of air, $\rho = 1.29 \times 10^{-18}\,\mathrm{kg/\mu m^3}$, $h = 2\,\mu\mathrm{m}$ in this paper. So, it can be obtained that the vibration frequency $f = \omega/2\pi$ should be much less than $1 \times 10^6\,\mathrm{Hz}$.

For the (c), air layer is relative thick, so Stokes flow model was applied [11]. The damp coefficient was

$$C_c = \mu\beta A \frac{\sinh(2\beta h) + \sin(2\beta h)}{\cosh(2\beta h) - \cos(2\beta h)},$$
$$\beta = \sqrt{\frac{\pi f}{\nu}} \tag{2.10}$$

where μ is viscosity coefficient of air, $\mu = 0.185 \times 10^{-10}\,\mathrm{kg/s/\mu m}$, f is vibration frequency of the resonator, ν is motion viscous ratio, $\nu = 0.157 \times 10^{-8}\,\mu\mathrm{m^2/s}$, A is the lower surface area of the movable finger structure, A_c is the sum of the fingers' side face area, d is the clearance

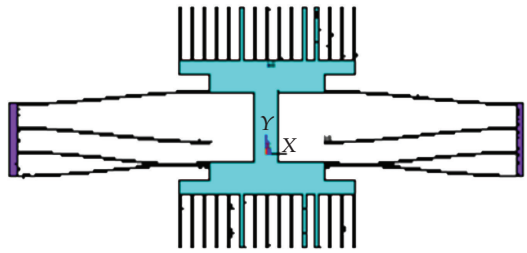

Figure 3: The first vibrational mode of microresonator.

between the microcomb and the base, g is the clearance between the fingers, h is the thickness of the finger. Then the whole damping is the summation of the three parts:

$$C = C_a + C_b + C_c = \frac{\mu A}{d} + \frac{\mu A_c}{g}\mu\beta A\frac{\sinh(2\beta h) + \sin(2\beta h)}{\cosh(2\beta h) - \cos(2\beta h)}. \tag{2.11}$$

3. Dynamic Characteristics Analysis of Faulted Micro-Comb Resonator

Movable structure adhesion and support beam crack are two typical faults of microcomb resonator. Adhesion indicates the movable part fixed, because the clearance in MEMS is very small, during the fabrication process, the movable part is easy to be blocked and stuck by microparticle mass, which leads to the needless structure mounting. The crack usually occurs in the support beam or fingers, which is induced by residual stress or repeated motion. Other defects, such as the mass and stiffness change or asymmetric distribution of the support beam caused by contamination during the fabrication process, perhaps does not bring on the beam cracks or broken, but affect the dynamic performance of the MEMS. In this paper, two typical faults are analyzed their effects on the dynamic performance of microcomb resonator.

3.1. Natural Characteristics of the Micro-Comb Structure

The structural parameters used in this paper are shown in Table 1. The dynamic performance of a microcomb includes natural frequencies, vibration amplitude, response time, quality factor, and so on. From the homogeneous equation of (2.1), by subspace iterative method, the first natural frequency and mode can be obtained, which is the structure's sensitivity work mode. The first natural frequency is $f_n = 11881\,\text{Hz}$, and the 1st mode is shown in Figure 3. For this structure, the damping coefficient can be obtained from (2.11), which is $C = 1.76 \times 10^{-7}\,\text{kg/s}$ at resonator frequency.

When offset voltage $V_p = 50\,\text{V}$ and driven alternating voltage $V_d = 25\sin(2\pi ft)\,\text{V}$ is loaded, where f is the driving frequency, the amplitude frequency response characteristics are analyzed, the maximal amplitude is $A_m = 12.785\,\mu\text{m}$ at natural frequency $f_n = 11881\,\text{Hz}$. The sensitivity of microcomb resonators is defined as the ratio of vibration amplitude of structure and the driven voltage, so at the natural frequency, the sensitivity $s = 0.5114\,\mu\text{m/V}$.

Table 1: The structural parameters of microcomb resonator.

Parameter	Size
Finger gap: g/μm	2.88
Finger length: l/μm	40.05
Finger width: w/μm	2
Gap of comb: c/μm	20.61
Beam length: b_l/μm	151
Beam width: b_w/μm	1.1
Thickness: h/μm	1.96
Area of the lower surface of the movable Finger structure: A/μm^2	5.1×10^3
Sum of the fingers' side face area: A_c/μm^2	2.35×10^3
Substrate gap: d/μm	2
Truss length: t_l/μm	78
Truss width: t_w/μm	13

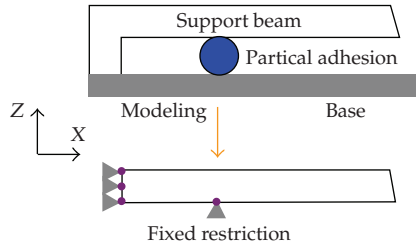

Figure 4: The model of adhesion fault.

3.2. *Analysis of Particle Adhesion Fault*

The most typical defect which can be encountered in the microcomb resonators is stiction of the suspended beams to the substrate surface. Stiction can mostly occur during MEMS processing (e.g., wet etching). During wet chemical etching, removal of a chip from the liquid etchant often pulls suspended parts towards the substrate surface where they remain stuck due to capillary forces and Van der Waals force. Once in contact, and even after the chip has been dried up, suspended parts may remain stuck due to different types of adhesion forces. In this case, the microresonator will be failure due to the movable part fixed. In this paper, another adhesion case caused by the exterior particle is considered, which will not lead to the failure of the resonator, so is easier to be neglected.

When the exterior particle comes into the structure, rests between the movable part and the fixed part, which will lead to the point adhesion due to the molecular force and so on. Electric particle will cause the resonator short circuit and failure. Insulative particle may not lead the structure entire failure, but may cause the dynamic characteristics change. In this section, the adhesion fault due to insulative particle is analyzed, we assume the particle is rigid, the movable part cannot move relative to the substrate at the adhesion point. Figure 4 shows the simple model of the resonator with an adhesion point.

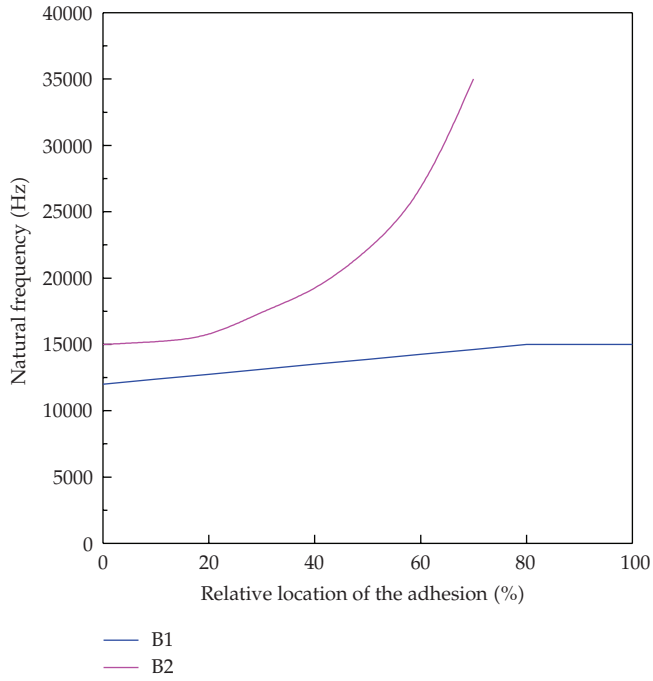

Figure 5: Natural frequencies change with the adhesive locations.

Support beam of the resonator is a folded symmetric structure, where B1 and B2 are two parallel beams of them, as shown in Figure 1(b). One end of B1 is fixed on the substrate. The adhesion at different location of B1 or B2 has different effect on the natural characteristics of the resonator.

Figure 5 shows that the natural frequency change with the location of adhesion, the abscissa is relative location of the adhesion. Where define relative location of adhesion at B1 beam as the ratio of distance from adhesion to the fixed end and the length of B1, and the relative location at B2 is the ratio of distance from adhesion to the folded end and the length of B2, as shown in Figure 1(b). It can be seen from Figure 5 that the natural frequency becomes higher due to the adhesion fault, and increases with the adhesion location ratio growing. Adhesion at B2 has more greatly effect on natural frequency than adhesion at B1. As the relative location ratio at B2 increases, the natural frequency increases more quickly.

Because the adhesion fault is difficult to be predicted in advance, the loaded voltage is usually kept on the faultless resonant frequency $f_n = 11881\,\text{Hz}$, which is called operating frequency. In case the adhesion fault occurs, driving frequency does not change, then the vibration amplitude (working amplitude) changes, lead to reduction of the sensitivity.

When offset voltage 50 V and driven alternating voltage of amplitude 25 V and frequency 11881 Hz is loaded, the relationship of sensitivity and the location of adhesion are shown in Figure 6. It can be seen that the adhesion fault makes the sensitivity lower. As the adhesion relative location ratio at B1 increases, the sensitivity reduces quickly. Adhesion fault at B2 makes the sensitivity reduces too, obviously the resonator is not working on the resonant state here. When the adhesion is located at 10% of B1, sensitivity $s = 0.4144\,\mu\text{m/V}$, however when it is located at 70% of B2, the sensitivity has reduced to $s = 0.0032\,\mu\text{m/V}$.

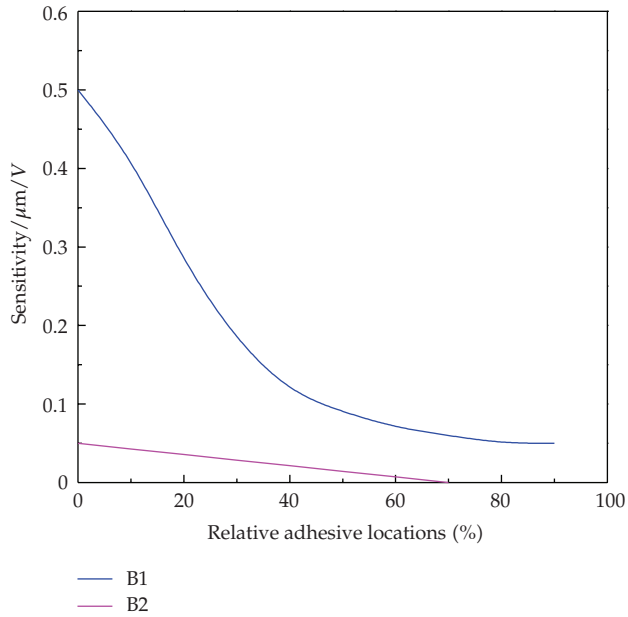

Figure 6: Sensitivity change with the adhesive locations.

3.3. Analysis of the Beam Crack Fault

Crack is a common fault in MEMS. Some microcrack influences not only on the structure performance, but also results in the structure failure when the crack expands with the motion. Beam structure is often used in microresonator. A crack could easily occur due to the stress concentration during fabrication process. In addition, during DRIE process, if the impurity adheres to the etching model, mass lack could occurred, which will cause such faults as crack or perforation.

In this paper, we only analyzed the support beam crack fault, because the support beam stiffness has crucial influence on the dynamic performance of the resonator. The beam crack is simplified as the square groove here. Based on Saint-Venant's Principle, the width of crack is set to $0.1\,\mu$m, which is much smaller than the length of support beam. The depth of crack is set to half of the thickness of the beam. The FEM mesh of cracked beam is shown in Figure 7. 4-node tetrahedral elements are applied here. Figure 8 shows the relationship of resonant frequency and the crack location. The curve for B1 and B2 are similar. The crack causes the resonant frequency lower. The crack located in the middle of B1 and B2 has fewer effect on the resonator frequency, but the crack located near the end of B1 or B2 has more effect on it. The frequency for B2 crack is somewhat higher than that in B1. Comparing with the adhesion fault, the beam crack fault has smaller influence on the resonator frequency. Figure 9 shows the relationship of sensitivity and the crack locations. It can be seen the crack fault causes the sensitivity to be lower, especially for the crack near beam end. When the crack is located in 10% of B1, sensitivity $s = 0.5072\,\mu$m/V, for crack located in 10% of B2, it is $s = 0.5091\,\mu$m/V. Comparing with the adhesion fault, crack has smaller effect on the resonator's dynamic performance.

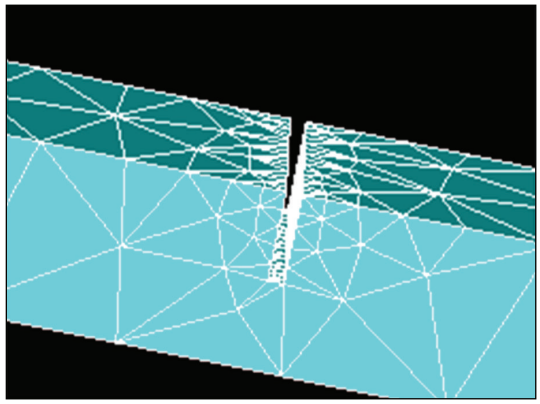

Figure 7: Support beam crack model with FEM.

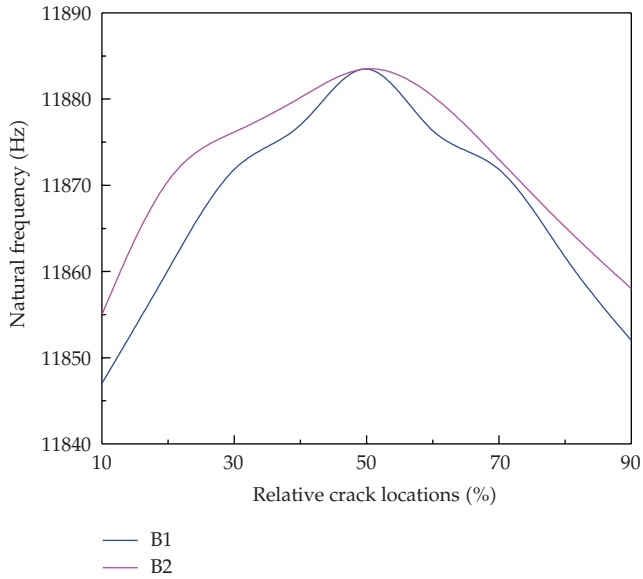

Figure 8: Natural frequencies change with the beam crack locations.

However, crack could cause the stress concentration, sometimes makes the beam broken, and leads to severity failure. Figure 10 shows the maximal stress along B1 and B2, at different crack location. The maximal stress is almost at the crack location. When the crack is located near the end, the maximal stress is highest, which is easy to cause the support beam broken.

4. Conclusion

In this paper, a microcomb resonator with faults was simulated, air damping was considered. The influence of faults on the dynamic performance of microresonator is analyzed. The results

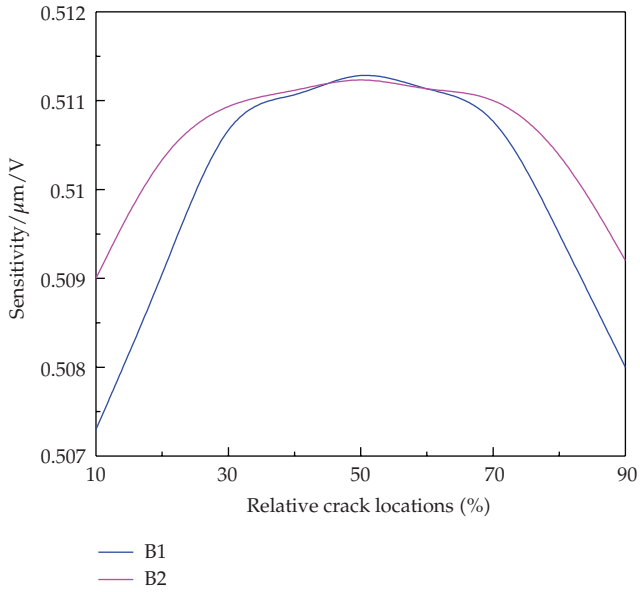

Figure 9: Sensitivity change with the crack locations.

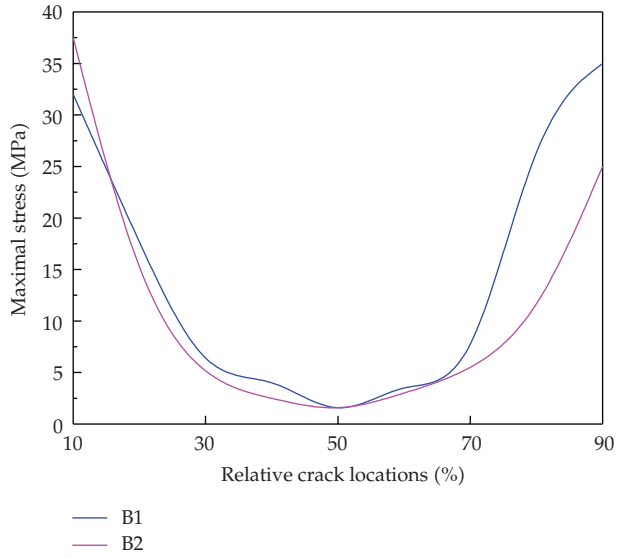

Figure 10: The maximal stresses change with the crack locations.

show that adhesion fault makes the frequency higher, while crack fault reduces the natural frequency. Both faults reduce the sensitivity. The adhesion fault has more obvious effect on the dynamic characteristics than the crack fault, However, if the crack is located near the end, the stress concentration at the crack location is highest, which is easy to cause the support beam broken.

Nomenclature

$[K]$: Structural stiffness matrix
$[M]$: Structural mass matrix
$[C]$: Air damping matrix
$\{u\}$: Node displacement vector
$\{F\}$: The electrostatic force vector
$\{E\}$: Electric field intensity vector
ω: Alternating frequency of electric field
V: Electric potential
ε: Dielectric coefficient of air, pF/μm
μ: Viscosity coefficient of air, kg/s/μm
ρ: Density of air, kg/μm^3
ν: Motion viscous ratio of air, μm^2/s
f: Vibration frequency of the microresonator, Hz
A: The lower surface area of the movable finger structure, μm^2
A_c: The sum of the fingers' side face area, μm^2
d: The clearance between the microcomb and the base, μm
g: The clearance between the fingers, μm
h: The thickness of the finger, μm
l: Finger length, μm
w: Finger width, μm
c: Gap of comb, μm
b_l: Beam length, μm
h: Thickness of comb structure, μm
t_l: Truss length, μm
t_w: Truss width, μm
V_p: Offset voltage, V
V_d: Driven alternating voltage, V
A_m: Maximal vibration amplitude, μm
s: Sensitivity of microcomb resonators, μm/V.

Acknowledgment

This research is supported by National Natural Science Foundation of China (Grant no. 50775121) and the National Natural Science Key Foundation of China (Grant no. 50730007).

References

[1] Kolpekwar, R. D. Blanton, and D. Woodilla, "Failure modes for stiction in surface-micromachined MEMS," in *Proceedings of IEEE International Test Conference (TC '98)*, pp. 551–556, IEEE Computer Society, Washington, DC, USA, October 1998.
[2] N. Deb and R. D. Blanton, "High-level fault modeling in surface-micromachined MEMS," in *Design, Test, Integration, and Packaging of MEMS/MOEMS*, vol. 4019 of *Proceedings of SPIE*, pp. 228–235, Paris, France, May 2000.
[3] R. Reichenbach, R. Rosing, A. Richardson, and A. Dorey, "Finite element analysis to support component level fault modelling for MEMS," in *Design, Test, Integration, and Packaging of MEMS/MOEMS*, vol. 4408 of *Proceedings of SPIE*, pp. 147–158, Cannes-Mandelieu, France, April 2001.
[4] Z. Chen, Y. Y. He, F. L. Chu, and J. Huang, "Dynamic characteristic analysis of the micro-structure with defects," *Chinese Journal of Mechanical Engineering*, vol. 40, no. 6, pp. 23–27, 2004.

[5] S. Mir, B. Charlot, and B. Courtois, "Extending fault-based testing to microelectromechanical systems," *Journal of Electronic Testing: Theory and Applications*, vol. 16, no. 3, pp. 279–288, 2000.
[6] W. C. Tang, T.-C. H. Nguyen, and R. T. Howe, "Laterally driven polysilicon resonant microstructures," *Sensors and Actuators*, vol. 20, no. 1-2, pp. 25–32, 1989.
[7] W. Huang and G. Y. Lu, "Analysis of lateral instability of in-plane comb drive MEMS actuators based on a two-dimensional model," *Sensors and Actuators A*, vol. 113, no. 1, pp. 78–85, 2004.
[8] I. V. Avdeev, M. R. Lovell, and D. Onipede Jr., "Modeling in-plane misalignments in lateral combdrive transducers," *Journal of Micromechanics and Microengineering*, vol. 13, no. 6, pp. 809–815, 2003.
[9] G. Zhou and P. Dowd, "Tilted folded-beam suspension for extending the stable travel range of comb-drive actuators," *Journal of Micromechanics and Microengineering*, vol. 13, no. 2, pp. 178–183, 2003.
[10] C. Young, P. P. Albert, and R. T. Howe, "Viscous damping model laterally oscillating microstructures," *Journal of Microelectromechanical Systems*, vol. 3, no. 2, pp. 81–87, 1994.
[11] W. Ye, X. Wang, W. Hemmert, D. Freeman, and J. White, "Air damping in laterally oscillating microresonators: a numerical and experimental study," *Journal of Microelectromechanical Systems*, vol. 12, no. 5, pp. 557–566, 2003.
[12] E. M. Lifshitz, *Fluid Mechanics*, Pergamon, New York, NY, USA, 2nd edition, 1989.